

3D/2D regularized CNN feature hierarchy for Hyperspectral image classification

Muhammad Ahmad, Manuel Mazzara, and Salvatore Distefano

Abstract—Convolutional Neural Networks (CNN) have been rigorously studied for Hyperspectral Image Classification (HSIC) and are known to be effective in exploiting joint spatial-spectral information with the expense of lower generalization performance and learning speed due to the hard labels and non-uniform distribution over labels. Several regularization techniques have been used to overcome the aforesaid issues. However, sometimes models learn to predict the samples extremely confidently which is not good from a generalization point of view. Therefore, this paper proposed an idea to enhance the generalization performance of a hybrid CNN for HSIC using soft labels that are a weighted average of the hard labels and uniform distribution over ground labels. The proposed method helps to prevent CNN from becoming over-confident. We empirically show that in improving generalization performance, label smoothing also improves model calibration which significantly improves beam-search. Several publicly available Hyperspectral datasets are used to validate the experimental evaluation which reveals improved generalization performance, statistical significance, and computational complexity as compared to the state-of-the-art models. The source code will be made available at <https://github.com/mahmad00>.

Index Terms—Beam-search; Label Smoothing; Hybrid Convolutional Neural Network (CNN); Hyperspectral Images Classification (HSIC).

I. INTRODUCTION

HYPERSPECTRAL Imaging (HSI) has been extensively utilized for many real-world applications [1]; for instance, Crop monitoring, vegetation coverage, precision agriculture, land resources, oil spills, water quality, meat adulteration [2], [3], adulteration in house hold products such as color adulteration detection in red chili [4], microbial spoilage and shelf-life of bakery products [5].

Thus, HSI Classification (HSIC) has received remarkable attention and intensive research results have been reported in the past few decades [6]. According to the literature, HSIC can be categorized into spatial, spectral, and spatial-spectral feature methods [7]. The spectral feature can be labeled as a primitive characteristic of HSI also known as spectral curve or vector whereas the spatial feature contains the relationship between the central pixel and its context which significantly uplifts the performance [8].

In the last few years, deep learning especially Convolutional Neural Network (CNN) has received widespread attention due to its ability to automatically learn non-linear features for classification, i.e., overcome the challenges of hand-crafted

features for classification. Moreover, it can jointly investigate the spatial-spectral information and such models can be categorized into two groups, i.e., single and two-stream, more information regarding single or two-stream methods can be found in [9]. This work explicitly investigate a single-stream method but in a combination of 3-D and 2-D layers.

Irrespective of the single or two-stream method, all deep learning frameworks are sensitive to the loss which needs to be minimized [10], [11]. Several classical works showed that the gradient descent to minimize cross-entropy performs better in terms of classification and has fast convergence, however, to some extent, leads to the overfitting. Several regularization techniques such as dropout, L1, L2, etc., have been used to overcome the overfitting issues together with several other exotic objectives performed exceptionally well than the standard cross-entropy [12]. Recently, a work [13] proposed a Label Smoothing (LS) technique that improves the accuracy significantly by computing cross-entropy with a weighted mixture of targets with uniform distribution instead of hard-coded targets.

Since then, LS has been known to improve the classification performance of deep models [14]. However, the original idea was used to improve the classification performance of only the inception model on ImageNet data [13]. However, since then, various image classification models (training models) have used LS [15], [16]. Though the LS technique is widely used trick to improve the classification performance and to speed up the convergence process, however, it has not been much explored for HSIC, and above all, it has not been much explored regarding when and why LS should work. This is due to, in HSIC, sometimes models learn to predict the training samples extremely confidently which is not good from a generalization point of view.

Therefore, this paper proposed an idea to enhance the generalization performance of a hybrid CNN for HSIC using soft labels that are a weighted average of the hard labels and uniform distribution over target labels. The proposed method helps to prevent Hybrid CNN from becoming over-confident. We empirically show that in improving generalization performance, LS also improves model calibration which significantly improves beam-search. Several publicly available Hyperspectral datasets are used to validate the experimental evaluation which reveals improved generalization performance, statistical significance, and computational complexity as compared to the state-of-the-art 2-D/3-D CNN models.

II. PROPOSED METHODOLOGY

Let us assume that the Hyperspectral data can be represented as $R^{(M \times N) \times B^*} = [r_1, r_2, r_3, \dots, r_S]^T$, where B^* be the total

arXiv:2104.12136v1 [cs.CV] 25 Apr 2021

M. Ahmad is with the Department of Computer Science, National University of Computer and Emerging Sciences, Islamabad, Chiniot-Faisalabad Campus, Chiniot 35400, Pakistan

M. Mazzara is with Innopolis University, Innopolis 420500, Russia

S. Distefano is with Dipartimento di Matematica e Informatica—MIFT, University of Messina, Messina 98121, Italy

number of bands and $(M \times N)$ are the samples per band belonging to Y classes and $r_i = [r_{1,i}, r_{2,i}, r_{3,i}, \dots, r_{B^*,i}]^T$ is the i^{th} sample in the Hyperspectral Data. Suppose $(r_i, y_i) \in (\mathcal{R}^{M \times N \times B^*}, \mathcal{R}^Y)$, where y_i is the class label of the i^{th} sample. Later instead of using the "hot encoding" in hybrid model, we introduce a smoothing technique $\mu(y|r_i)$. Thus the new ground truths (r_i, y_i) would be:

$$p'(y|r_i) = (1 - \varepsilon)p(y|r_i) + \varepsilon\mu(y|r_i) \quad (1)$$

$$f(x) = \begin{cases} 1 - \varepsilon + \varepsilon\mu(y|r_i) & \text{if } y = y_i \\ \varepsilon\mu(y|x_i) & \text{otherwise} \end{cases} \quad (2)$$

where $\varepsilon \in [0, 1]$ is a weight factor, and note that $\sum_{y=1}^Y p'(y|r_i) = 1$. These new ground truths has been used in loss function instead of hot-encoding.

$$L' = - \sum_{i=1}^{M \times N} \sum_{y=1}^Y p'(y|r_i) \log q_\theta(y|r_i) \quad (3)$$

$$L' = - \sum_{i=1}^{M \times N} \sum_{y=1}^Y [(1 - \varepsilon)p(y|r_i) + \varepsilon\mu(y|r_i)] \log q_\theta(y|r_i) \quad (4)$$

$$L' = \sum_{i=1}^{M \times N} \left\{ (1 - \varepsilon) \left[- \sum_{y=1}^Y p(y|r_i) \log q_\theta(y|r_i) \right] + \varepsilon \left[- \sum_{y=1}^Y \mu(y|x_i) \log q_\theta(y|r_i) \right] \right\} \quad (5)$$

$$L' = \sum_{i=1}^{M \times N} \left[(1 - \varepsilon)H_i(p, q_\theta) + \varepsilon H_i(\mu, q_\theta) \right] \quad (6)$$

One can observe that each ground truth, the loss contribution is a mixture of entropy between predicted distribution ($H_i(p, q^\theta)$) and the hot-encoding, and the entropy between the predicted distribution ($H_i(\mu, q^\theta)$) and the noise distribution. While training, $H_i(p, q^\theta) = 0$ if the model learns to predict the distribution confidently, however, $H_i(\mu, q^\theta)$ will increase dramatically. To overcome this phenomenon, we used a regularizer $H_i(\mu, q^\theta)$ to prevent the model from predicting too confidently. In practice, $\mu(y|r)$ is a uniform distribution that does not dependant on Hyperspectral Data. That is to say $\mu(y|r) = \frac{1}{Y}$. The ultimate network is trained for 50 epochs using a mini-batch size of 256 without any batch normalization and data augmentation. In a nutshell, the details of 3D/2D convolutional layers and kernels are as follows: $3D_conv_layer_1 = 8 \times 5 \times 5 \times 7 \times 1$ i.e. $K_1^1 = 5, K_2^1 = 5$ and $K_3^1 = 7$. $3D_conv_layer_2 = 16 \times 5 \times 5 \times 5 \times 8$ i.e. $K_1^2 = 5, K_2^2 = 5$. $K_3^2 = 5$. $3D_conv_layer_3 = 32 \times 3 \times 3 \times 3 \times 16$ i.e. $K_1^3 = 3, K_2^3 = 3$ and $K_3^3 = 3$. $3D_conv_layer_4 = 64 \times 3 \times 3 \times 3 \times 32$ i.e. $K_1^3 = 3, K_2^3 = 3$ and $K_3^3 = 3$. $2D_conv_layer_5 = 128 \times 3 \times 3 \times 64$ i.e. $K_1^2 = 3$ and $K_2^2 = 3$. Three 3D convolutional layers are employed to increase the number of spectral-spatial feature maps and one 2D convolutional layer is used to discriminate the spatial features within different spectral bands while preserving the

spectral information. Initially, the weights are randomized and then optimized using back-propagation with the Adam optimizer by using the loss function presented in equation 6. Further details regarding the Hybrid CNN architecture in terms of types of layers, dimensions of output feature maps and number of trainable parameters can be found in [6].

III. EXPERIMENTAL SETTINGS AND RESULTS

The experiments have been conducted on two real HSI datasets, namely, Indian Pines (IP), and Pavia University (PU). These datasets are acquired by two different sensors i.e, Reflective Optics System Imaging Spectrometer (ROSIS) and Airborne Visible/Infrared Imaging Spectrometer (AVIRIS) [6]. The experimental results explained in this work have been obtained through Google Colab [17] which is an online platform to execute any python environment while having a good internet speed to execute the code. Google Colab provides the option to execute many versions of python, Graphical Process Unit (GPU), upto 358+ GB of cloud storage, and upto 25 GB of Random Access Memory (RAM).

In all the experiments, the initial size of the train/validation/test sets is set to 25%/25%/50% to validate the proposed model as well as several other state-of-art-deep models. The comparative methods include AlexNet [18], LeNet [19], 2D CNN [20], and 3D CNN [21] models. Moreover, the following accuracy metrics have been conducted to validate the claims made in this manuscript. The accuracy metrics include Kappa (κ)¹, Average (AA)², and Overall (OA)³. All these metrics are computed using the following equations.

$$Kappa (\kappa) = \frac{P_o - P_e}{1 - P_e} \quad (7)$$

where

$$P_e = P^+ + P^-$$

$$P^+ = \frac{TP + FN}{TP + FN + FP + TN} \times \frac{TP + FN}{TP + FN + FP + TN}$$

$$P^- = \frac{FN + TN}{TP + FN + FP + TN} \times \frac{FP + TN}{TP + FN + FP + TN}$$

$$P_o = \frac{TP + TN}{TP + FN + FP + TN}$$

$$Overall (OA) = \frac{1}{K} \sum_{i=1}^K TP_i \quad (8)$$

where TP and FP are true and false positive, TN and FN are true and false negative, respectively. For fair comparison purposes, the learning rate for all these models including hybrid models is set to 0.001, Relu as the activation function

¹ κ is known as a statistical metric that considered the mutual information regarding a strong agreement among classification and ground-truth maps

²AA represents the average class-wise classification performance

³OA is computed as the number of correctly classified examples out of the total test examples

for all layers except the output layer on which Softmax is used, patch size is set of 15, and for all the experiments, 15 most informative bands have been selected using principal component analysis to reduce the computational load. The convergence accuracy and loss of our proposed pipeline and all other competing methods for 50 epochs is presented in Figure 1. From loss and accuracy curves, one can conclude that the smoothing has faster convergence than the model without convergence.

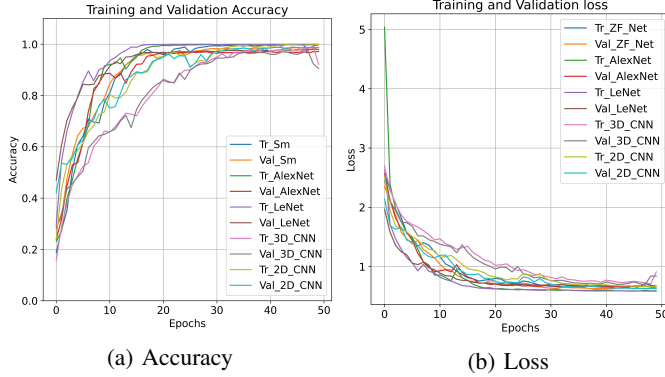


Fig. 1: Accuracy and Loss for Training and Validation sets on Indian Pines for 50 epochs.

A. Indian Pines

Indian pines (IP) dataset is acquired using AVIRIS sensor over the northwestern Indiana test site. IP data consist of 145×145 spatial dimensions and 224 spectral dimensions with total of 16 classes in which all are not mutually exclusive. Some of the water absorption bands are removed and the remaining 200 bands are used for the experimental process. This data is consists of 2/3 agriculture, 1/3 forest, and other vegetation. Less than 5% of total coverage consists of crops that are in an early stage of growth. Building, low-density housing, two dual-lane highway, small roads, and a railway line are also a part of it. Further details about the experimental datasets can be found at [22]. Table I and Figure 2 presents in-depth comparative accuracy analysis on the IP dataset.

TABLE I: **Indian Pines**: Performance analysis of different state-of-the-art models. The higher accuracies are emphasised.

Class	Train/Val/Test	2D	3D	AlexNet	LeNet	WoS	WS
Alfalfa	11/12/23	100	91.3043	95.6521	82.6086	100	100
Corn-notill	357/357/714	98.3193	93.5574	97.3389	97.0588	98.4593	98.8795
Corn-mintill	207/208/415	99.5180	66.7469	98.3132	99.5180	99.5180	99.5180
Corn	59/59/118	94.0677	90.6779	93.2203	99.1525	100	100
Grass-pasture	121/121/242	98.3471	97.1074	96.2809	94.2148	95.0413	96.2809
Grass-trees	182/183/365	98.9041	97.5342	98.3561	98.9041	99.4520	99.7260
Grass-mowed	7/7/14	92.8571	92.8571	100	100	92.8571	100
Hay-windrowed	119/120/239	100	100	100	100	100	100
Oats	5/5/10	70	0	100	70	100	100
Soybean-notill	243/243/486	98.5596	82.3045	93.6213	99.3827	97.9423	97.9423
Soybean-mintill	614/614/1228	99.6742	92.4267	97.8013	99.9185	99.7557	99.8371
Soybean-clean	148/149/297	97.6430	98.6531	96.9696	95.2861	98.3164	99.6632
Wheat	51/51/102	99.0196	98.0392	100	99.0196	99.0196	100
Woods	316/317/633	99.8420	99.3680	99.5260	98.8941	99.2101	99.8420
Buildings	96/97/193	99.4818	90.6735	100	91.1917	100	99.4818
Stone-Steel	23/23/46	100	97.8260	100	93.4782	100	100
Training Time		55.6695	250.1662	919.5566	61.8763	250.1622	248.5993
Test Time		1.4897	4.0402	5.6891	1.2752	4.6499	3.9997
Overall Accuracy		98.9463	91.5707	97.6585	98.14634	98.9853	99.2975
Average Accuracy		98.7980	86.8173	97.9425	94.9142	98.7232	99.3869
Kappa (κ)		96.6396	90.3561	97.3312	97.8853	98.8430	99.1990

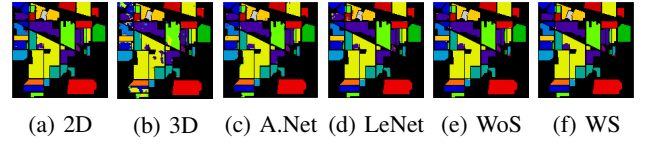


Fig. 2: **Indian Pines**: Classification accuracy: Fig. 2a: 2D-CNN = 98.94%, Fig. 2b: 3D CNN = 91.57%, Fig. 2c: AlexNet = 97.65%, Fig. 2d: LeNet = 98.14%, Fig. 2e: WoS (Hybrid net without Smoothing) = 98.98%, and Fig. 2f WS (with Smoothing) = **99.29%**.

B. Pavia University

Pavia University (PU) dataset acquired using Reflective Optics System Imaging Spectrometer (ROSIS) optical sensor over Pavia in northern Italy. PU dataset is distinguished into 9 different classes. PU consists of 610×610 spatial samples per spectral band and 103 spectral bands with a spatial resolution of 1.3m. Further details about the experimental datasets can be found at [22]. Table II and Figure 3 presents in-depth comparative accuracy analysis on the IP dataset.

TABLE II: **Pavia University**: Performance analysis of different state-of-the-art models. The higher accuracies are emphasised.

Class	Train/Val/Test	2D	3D	AlexNet	LeNet	WoS	WS
Asphalt	1658/1658/3316	100	100	98.9143	100	100	100
Meadows	4662/4662/9324	100	99.9892	100	100	100	100
Gravel	524/525/1049	99.5233	99.3326	95.5195	99.4280	99.5233	99.6186
Trees	766/766/1532	99.6736	100	98.8250	99.7389	100	100
Painted	336/337/673	100	100	100	100	100	100
Soil	1257/1257/2514	100	100	99.9602	100	100	100
Bitumen	332/333/665	100	100	99.6992	100	100	100
Bricks	920/921/1841	99.8913	99.8913	97.9359	100	99.8913	99.8913
Shadows	237/237/474	99.3670	99.5780	98.5232	99.7890	99.7890	100
Training Time		296.0174	1145.9233	4716.4900	308.6389	1143.5753	1143.4996
Test Time		5.7400	14.8634	24.1701	4.5054	15.0601	15.5904
Overall Accuracy		99.9298	99.9438	99.3033	99.9485	99.9625	99.9719
Average Accuracy		99.8283	99.8657	98.8197	99.8839	99.9115	99.9455
Kappa (κ)		99.9070	99.9256	99.0768	99.9318	99.9504	99.9628

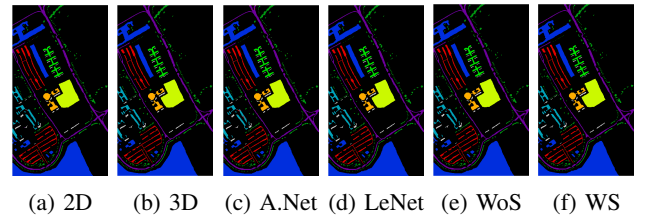


Fig. 3: **Pavia University**: Classification accuracy: Fig. 3a: 2D-CNN = 99.9070%, Fig. 3b: 3D CNN = 99.9256%, Fig. 3c: AlexNet = 99.0768%, Fig. 3d: LeNet = 99.9318%, Fig. 3e: WoS (Hybrid net without Smoothing) = 99.9504%, and Fig. 3f: WS (with Smoothing) = **99.9628%**.

IV. CONCLUSION

The paper proposed a 3D/2D regularized CNN feature hierarchy for HSIC, in which the loss contribution is considered as a mixture of entropy between a predicted distribution and the hot-encoding, and the entropy between the predicted and noise distribution. Several other regularization techniques (e.g., dropout, L1, L2, etc.) have also been used, however, these techniques to some extent, lead to predicting the samples

extremely confidently which is not good from a generalization point of view. Therefore, this work proposed the use of an entropy-based regularization process to improve the generalization performance using soft labels. These soft labels are the weighted average of the hard labels and uniform distribution over entire ground truths. The entropy-based regularization process prevents CNN from becoming over-confident while learning and predicting thus improves the model calibration and beam-search. Extensive experiments have confirmed that the proposed pipeline outperformed several state-of-the-art methods.

REFERENCES

- [1] A. Alcolea, M. E. Paoletti, J. M. Haut, J. Resano, and A. Plaza, "Inference in supervised spectral classifiers for on-board hyperspectral imaging: An overview," *Remote Sensing*, vol. 12, no. 3, p. 534, 2020.
- [2] H. Ayaz, M. Ahmad, A. Sohaib, M. N. Yasir, M. A. Zaidan, M. Ali, M. H. Khan, and Z. Saleem, "Myoglobin-based classification of minced meat using hyperspectral imaging," *Applied Sciences*, vol. 10, no. 19, p. 6862, 2020.
- [3] H. Ayaz, M. Ahmad, M. Mazzara, and A. Sohaib, "Hyperspectral imaging for minced meat classification using nonlinear deep features," *Applied Sciences*, vol. 10, no. 21, p. 6862, 2020.
- [4] M. H. Khan, S. Zainab, M. Ahmad, A. Sohaib, H. Ayaz, and M. Mazzara, "Hyperspectral imaging for color adulteration detection in red chili," *Applied Sciences*, vol. 10, no. 17, p. 5955, 2020.
- [5] Z. Saleem, M. H. Khan, M. Ahmad, A. Sohaib, H. Ayaz, and M. Mazzara, "Prediction of microbial spoilage and shelf-life of bakery products through hyperspectral imaging," *IEEE Access*, vol. 8, pp. 176 986–176 996, 2020.
- [6] M. Ahmad, S. Shabbir, R. A. Raza, M. Mazzara, S. Distefano, and A. M. Khan, "Hyperspectral image classification: Artifacts of dimension reduction on hybrid cnn," *arXiv preprint arXiv:2101.10532*, 2021.
- [7] J. Wang, R. Huang, S. Guo, L. Li, M. Zhu, S. Yang, and L. Jiao, "Nas-guided lightweight multiscale attention fusion network for hyperspectral image classification," *IEEE Transactions on Geoscience and Remote Sensing*, pp. 1–14, 2021.
- [8] S. Shabbir and M. Ahmad, "Hyperspectral image classification—traditional to deep models: A survey for future prospects," *arXiv preprint arXiv:2101.06116*, 2021.
- [9] S. Jia, S. Jiang, Z. Lin, N. Li, M. Xu, and S. Yu, "A survey: Deep learning for hyperspectral image classification with few labeled samples," *Neurocomputing*, vol. 448, pp. 179–204, 2021. [Online]. Available: <https://www.sciencedirect.com/science/article/pii/S0925231221004033>
- [10] D. E. Rumelhart, G. E. Hinton, and R. J. Williams, *Learning Representations by Back-Propagating Errors*. Cambridge, MA, USA: MIT Press, 1988, p. 696–699.
- [11] H. Sha, M. Al Hasan, and G. Mohler, "Learning network event sequences using long short-term memory and second-order statistic loss," *Stat. Anal. Data Min.*, vol. 14, no. 1, p. 61–73, Jan. 2021. [Online]. Available: <https://doi.org/10.1002/sam.11489>
- [12] H. Bi, R. Santos-Rodriguez, and P. Flach, "Polar image classification via robust low-rank feature extraction and markov random field," in *IGARSS 2020 - 2020 IEEE International Geoscience and Remote Sensing Symposium*, 2020, pp. 708–711.
- [13] C. Szegedy, V. Vanhoucke, S. Ioffe, J. Shlens, and Z. Wojna, "Rethinking the inception architecture for computer vision," 06 2016.
- [14] C. Zhang and M. Han, "Multi-feature hyperspectral image classification with $l_{2,1}$ norm constrained joint sparse representation," *International Journal of Remote Sensing*, vol. 42, no. 12, pp. 4789–4808, 2021. [Online]. Available: <https://doi.org/10.1080/01431161.2021.1890854>
- [15] E. Real, A. Aggarwal, Y. Huang, and Q. V. Le, "Regularized evolution for image classifier architecture search," *Proceedings of the AAAI Conference on Artificial Intelligence*, vol. 33, no. 01, pp. 4780–4789, Jul. 2019. [Online]. Available: <https://ojs.aaai.org/index.php/AAAI/article/view/4405>
- [16] B. Zoph, V. Vasudevan, J. Shlens, and Q. V. Le, "Learning transferable architectures for scalable image recognition," *CoRR*, vol. abs/1707.07012, 2017. [Online]. Available: <http://arxiv.org/abs/1707.07012>
- [17] T. Carneiro, R. V. M. Da Nóbrega, T. Nepomuceno, G.-B. Bian, V. H. C. De Albuquerque, and P. P. Reboucas Filho, "Performance analysis of google colabouratory as a tool for accelerating deep learning applications," *IEEE Access*, vol. 6, pp. 61 677–61 685, 2018.
- [18] S. Mei, X. Chen, Y. Zhang, J. Li, and A. Plaza, "Accelerating convolutional neural network-based hyperspectral image classification by step activation quantization," *IEEE Transactions on Geoscience and Remote Sensing*, pp. 1–12, 2021.
- [19] Y. Yuan, C. Wang, and Z. Jiang, "Proxy-based deep learning framework for spectral-spatial hyperspectral image classification: Efficient and robust," *IEEE Transactions on Geoscience and Remote Sensing*, pp. 1–15, 2021.
- [20] H.-C. Li, S.-S. Li, W.-S. Hu, J.-H. Feng, W.-W. Sun, and Q. Du, "Recurrent feedback convolutional neural network for hyperspectral image classification," *IEEE Geoscience and Remote Sensing Letters*, pp. 1–5, 2021.
- [21] M. Ahmad, A. M. Khan, M. Mazzara, S. Distefano, M. Ali, and M. S. Sarfraz, "A fast and compact 3-d cnn for hyperspectral image classification," *IEEE Geoscience and Remote Sensing Letters*, pp. 1–5, 2020.
- [22] *Hyperspectral Datasets Description*, 2021 (accessed 2020-04-01), http://www.ehu.es/ccwintco/index.php/Hyperspectral_Remote_Sensing_Scenes.